


Flares and their echoes can help distinguish photon rings from black holes with space-Earth very long baseline interferometry

A. Andrianov¹,¹ S. Chernov,¹ I. Girin,¹ S. Likhachev,¹ A. Lyakhovets¹,¹ and Yu. Shchekinov^{1,2}

¹*Astro Space Center, Lebedev Physical Institute, 84/32 Profsoyuznaya street, 117997, Moscow, Russia*

²*Raman Research Institute, C. V. Raman Ave., Sadashivanagar, Bengaluru 560080, India*

 (Received 1 December 2021; accepted 25 February 2022; published 22 March 2022)

Photon rings near the edge of a black hole shadow are supposed to be a unique tool to validate general relativity and provide reliable measurements of principal black hole parameters: spin and mass. Such measurements are possible though only for nearby supermassive black holes (SMBH) with space-Earth very long baseline interferometry (S-VLBI) in the submillimeter wavelength range. For subrings to be distinguished S-EVLBI observations with long baselines at the Lagrangian Sun-Earth L2 libration point are needed. However, the average fluxes of nearby SMBH: Sagittarius A* (Sgr A*) and M87* — $F_\nu \sim 1$ Jy, are still insufficient to detect the signal from the photon rings with even such long baselines. We argue that only manifestations of flares in the submillimeter waveband in their accretion disks can reveal observable signals from the photon rings with the S-EVLBI at L2. Such observations will become possible within the planned joint program of the *Event Horizon Telescope* (EHT) and *Millimetron Space Observatory* (MSO), and within the planned *next generation EHT* (ngEHT) project. Two different observational tests for photons rings are discussed. The first one involves observations of a time series of responds from subsequent subrings as can be seen in a 1D visibility function within the join EHT-MSO configuration, the second one—measurements of an increase of the angle between subsequent subrings in the 2D VLBI image which can be obtained within the ngEHT project.

DOI: [10.1103/PhysRevD.105.063015](https://doi.org/10.1103/PhysRevD.105.063015)

I. INTRODUCTION

The Event Horizon Telescope Collaboration (EHTC) has approached the very vicinity of the supermassive black hole (SMBH)—its shadow, in the center of galaxy M87 with the highest angular resolution of $\sim 25 \mu\text{as}$ available within ground-based very-long-baselines (VLBI) technique [1–6]. This opens a new era of studying spacetime geometry and plasma processes under very strong gravitational forces in the area neighboring the SMBH horizon. The primary goal of the EHT experiment was to directly observe the black hole “image,” i.e., the shadow around the black hole, and to see whether the spacetime geometry is described by the Kerr metric as follows from Einstein general relativity and satisfies as such the “no-hair theorem” [see discussion in [7]]. In April 2017, a critical experiment at $\lambda = 1.3$ mm revealed the shadow of the angular size $\theta_{\text{shadow}} \simeq 45 \mu\text{as}$ as predicted [8], and led the EHTC to conclude that a metric of a supermassive black hole in the center of galaxy M87 is consistent with the Kerr metric [6], and with the mass close to the one inferred early from stellar kinematics in the central zone of galaxy M87 [9].

A complementary approach to test general relativity has been recently suggested by [10]. When passing around the black hole close to the innermost stable circular orbit (ISCO) photons from accreting plasma are captured onto a

quasistable orbit [11,12] where they can round over the ISCO a few times. Those reaching the observer screen leave on it a bright photon ring consisting of weaker embedded subrings, that imprint characteristics of spacetime metrics in which they have been formed. Thus they represent an informative tool for a quantitative characterization of the metric, and provide an authentic validation of Einstein general relativity [10]. Observationally this information is encoded in a 1D visibility function consisting of a hierarchy of responses from subsequent photon subrings. Each ring is formed by light that was emitted by the accretion disk and reached the observer’s screen along n half-orbits trajectories around the black hole. Those photons that come directly from the accretion disk are assigned $n = 0$. The photons lensed along one half-orbit trajectory are focused onto the *leading* ring with $n = 1$. As stressed by Ref. [10] higher order subrings with $n > 1$ unambiguously encode parameters of the black hole metric and can serve a unique tool for studying gravity theories. The higher the order of a subring n the slower the amplitude of its 1D visibility function declines on larger VLBI base lengths. For the visibility functions of $n = 2$ and $n = 3$ subrings to exceed contributions from the disk $n = 0$ and the leading ring $n = 1$, the baseline has to be increased beyond $u(\lambda) \gtrsim 3 \times 10^{11} \lambda$ (see Fig. 5 in Ref. [10]). Therefore, observations of the rings $n = 2$ and $n = 3$ in the submillimeter waverange

suggest baselines equivalent to the distance between Earth and the Lagrangian libration point L2. However, with the central flux density of the order ~ 1 Jy in the nearby SMBH—Sgr A* and M87*, and consequently photon subrings are to have only ~ 100 μ Jy (1σ level) at baselines ~ 1 T λ at the frequency $\nu = 230$ GHz in the L2 point, [see Fig. 5 below in Sec. IV A]. Such a flux seems to be insufficient for detection with the planning MSO-EHT configuration at $\nu = 230$ GHz with a bandwidth of 16 GHz and the ultimate 1σ detection limit ~ 0.2 mJy (see discussion in Ref. [13]).

A possible solution of this issue can be sought in utilizing enhanced brightness of submillimeter (submm) flares on the accretion disk, via extracting similarities in time series in the main flare and its reflections on the photon subrings. Submillimeter flares are known to accompany bright x-ray and near-infrared flares with time delays of ~ 20 minutes [14] to a few hours (see review and references in Ref. [15]). A month-long delay between the NIR and submm flares has occurred recently (June 2019), as described by [16]. From comparison of its structure function with one of other similar flares taken place during the period 2002–2017, Ref. [16] concluded that the most likely source of these flarings is magnetic reconnection. Numerical simulations performed by several research groups indicate that magnetic reconnections preferentially occur in the innermost regions of accretion disks and even close to jet boundary [17,18]. This circumstance makes the submm wavebands a unique instrument for studying space-time metric near black holes, along with the properties of relativistic plasma in extreme conditions close to the inner boundary of accretions disks and near the jet core. In the current paper we analyze this possibility. The paper is organized as follows. Section II describes a simplified model of geometrically thin disk and the black hole shadow. Section III considers the effects of the black hole spin on the photon rings that appear in our simplified model in the relationship between the parameters a , the spin, and θ_{los} , its inclination to the line of sight. Section IV describes a simplified model of a flare in the accretion disk and analyzes its interferometric response in form of a time-dependent visibility function on a long MSO-EHT baseline. In addition, we analyze a feasibility of VLBI imaging of a flare with its echoes in photon rings for Sgr A* with the ngEHT ground-based network. Section V contains conclusions.

II. BLACK HOLE SHADOW MODEL

In this paper we use a simplified toy model of geometrically thin disk around a Kerr black hole with the mass M and angular momentum $J = aM$ ($0 \leq a \leq M$) (see Fig. 1). The inner disk radius is set to $r_{\text{in}} = 8r_g$, $r_g = GM/c^2$, the outer disk radius is $r_{\text{out}} = 45r_g$. In this simplified toy model we assume that the disk radiates uniformly (each pixel has equal brightness) and isotropically. The spacetime

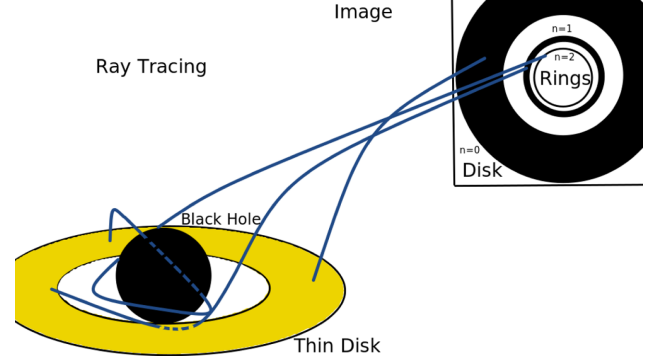


FIG. 1. A simplified toy model (not to scale) of a geometrically thin disk around a Kerr black hole and the image of photon rings in the observer plane. The inner disk radius is set to $r_{\text{in}} = 8r_g$, $r_g = GM/c^2$, the outer disk radius is $r_{\text{out}} = 45r_g$. The resulting image on the observer’s screen includes an image of the accretion disk ($n = 0$) and images of the photon rings ($n = 1, 2, 3$).

metric as described in Kerr-Schild coordinates with $G = c = 1$ is [19–22]

$$\begin{aligned} g_{\mu\nu} &= \eta_{\mu\nu} + f k_\mu k_\nu \\ f &= \frac{2Mr}{\Sigma}, \quad \Sigma = \frac{r^4 + a^2 z^2}{r^2} \\ k_\mu &= (1, k_x, k_y, k_z) \\ &= \left(1, \frac{rx + ay}{r^2 + a^2}, \frac{ry - ax}{r^2 + a^2}, \frac{z}{r} \right) \end{aligned} \quad (1)$$

where k^μ is the wave vector, r is defined by

$$\frac{x^2 + y^2}{r^2 + a^2} + \frac{z^2}{r^2} = 1. \quad (2)$$

The “null” geodesics for photon trajectories are described by

$$g_{\mu\nu} \frac{dx^\mu}{d\lambda} \frac{dx^\nu}{d\lambda} = 0, \quad (3)$$

with $g_{\mu\nu}$ from Eq. (1), and $\mu, \nu = 0, 1, 2, 3$, λ being affine parameter.

For numerical integration we can write Eq. (3) as a system of eight coupled first-order equations:

$$\begin{aligned} \frac{dx^\alpha}{d\lambda} &= k^\alpha \\ \frac{dk^\alpha}{d\lambda} &= -\Gamma_{\mu\nu}^\alpha k^\mu k^\nu \end{aligned} \quad (4)$$

where $\Gamma_{\mu\nu}^\alpha$ are the Christoffel symbols.

Let us consider a distant observer whose line-of-sight inclination angle with respect to the black-hole rotation axis

is θ_{los} . The vertical axis of the observer's image plane β is directed toward the projection of the black hole spin provided $\theta_{\text{los}} \neq 0$. On this plane, α is the impact parameter perpendicular to β [23]. For obtaining image on the observer's screen we apply the backward ray tracing for each image pixel (α, β) . The initial wave vector k is directed to the center of the black hole—the point with coordinates $(0,0,0)$. In numerical calculations the distance of the observer's screen from the BH is set to $40r_g$. For each image pixel, Eqs. (4) are solved with the Runge-Kutta 4-order integration method.

III. ANGULAR DISPLACEMENTS OF THE RINGS

Figure 1 illustrates possible photon trajectories that form the photon rings in our model. As mentioned in Sec. I the photons coming directly from the disk form its image on the observer's screen, those bent by lensing onto the one-half orbit trajectory $n = 1$ are focused into the leading ring, whereas $n > 1$ photons form higher order subrings.

Fluxes transmitted to subsequent photon rings depend on the accretion flow geometry, radiating plasma properties, and the path length through the emitting plasma [10,24]. General relativity dictates that relative contributions of subsequent rings are predominantly determined by the BH spin and its inclination to the observer. As the photon rings collect photons from wide areas in the disk they are brighter for higher n , however the total flux in a given ring decreases with n . For a Schwarzschild BH, the next order photon ring $n + 1$ carries only 4% of the total flux in the previous n ring [12,24]. For $a/M \sim 1$ and the inclination angle θ_{los} of $\sim 17^\circ$ it can be of $\sim 13\%$ [10]. In our simplified model with the geometrically thin uniform disk this parameter is $\sim 10\%$.

Figure 2 shows the modelled angular brightness distribution on the disk $I(\phi)$ and its projection onto the image plane. We color the disk white to brown clockwise starting from the direction coincident with the spin projection in the image plane as shown in Fig. 2. Where $\theta_{\text{los}} = 0$ and $a = 0$, as in the upper left subimage, the edge between brown and white is fixed along α -axis. In this case ($\theta_{\text{los}} = 0, a = 0$), the on-disk color pattern mapped onto the photon ring turns clockwise by $\delta\phi_{\text{obs}} = 180^\circ$ [12,25], again from white to brown. The panels in the upper row, left to right, correspond to the spin increase from $a = 0$ to $a = 1.0$ with increment $\delta a = 0.5$, the color pattern turns accordingly by $\delta\phi \approx 25^\circ\delta a$, in addition to $\delta\phi_{\text{obs}} = 180^\circ$. As the inclination θ_{los} increases the color pattern angle ϕ grows $\delta\phi(a, \theta_{\text{los}})$, as can be derived by solving numerically Eq. (4), or analytically from Eqs. (7b), (8c), and (8d) in [25]. Detection of bright sporadic flares (and their echoes in the photon rings) on the VLBI images can be utilized to distinguish photon rings and reveal the angular correspondence between events on the disk and in rings. For Sgr A*, this possibility is shown in Sec. IV C.

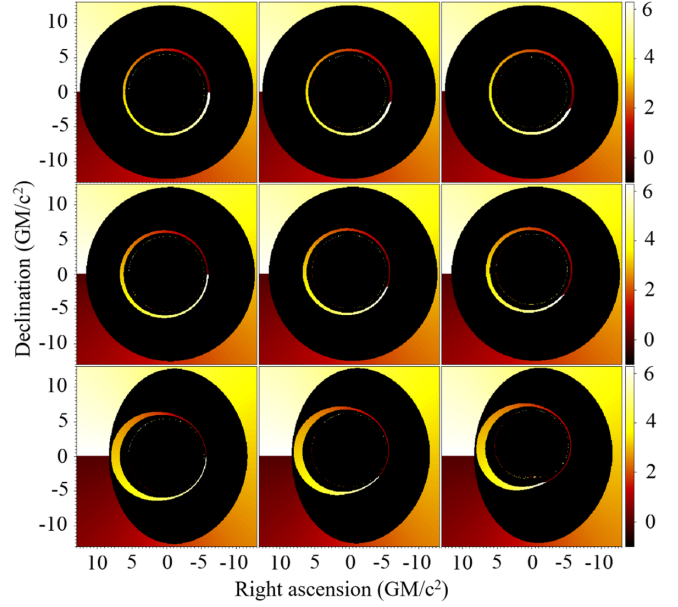


FIG. 2. Photon rings from a thin disk are color coded white to brown depending on the angle from a given direction (coincident with β -axis—the spin projection onto the observer's screen). The disk projection on the leading photon ring is similarly coded. The upper row shows the disk and the leading photon ring for a black hole with angular momentum along the sight line $\theta_{\text{los}} = 0$, $a = 0.0, 0.5, 1.0$ from left to right; the middle row shows the same but for angular momentum inclined to the sight line by $\theta_{\text{los}} = 17^\circ$, and the lower row is for $\theta_{\text{los}} = 45^\circ$. The turn of the disk pattern map reflected on the photon ring is clearly seen from (i) increase in a shown on panels from left to right, and (ii) increase in the spin inclination to the line of sight θ_{los} —panels from top to bottom.

IV. TIME VARIABILITY IN THE DISK

Bright sporadic flares (and their sequences) can be utilized to distinguish photon rings from the main crescent image of the disk. Let us assume a spot-like flare at time point t_f and at a given location in the disk. On the observer's plane the flare first responds in the crescent image, and after time delay $\Delta t_f \sim a \text{ few } \times n\pi r_g/c$ repeats its respond in the projection onto the leading photon ring ($n = 1$), and subsequently onto subrings with higher n . Overall, each of such flares can be reflected onto subsequent photon rings with a sequence of subflares as illustrated in Fig. 3. The geometric shapes of a flare and its projections onto the first ring are shown as red spots in the right panel of Fig. 3 and have been numerically obtained by backward ray tracing of the geometrically thin accretion disk model (See Sec. II). Note that the flare responds on the rings are brighter because they are localized in a much narrower area on the rings contrary to its spread respond on the crescent. Submm flares are apparently very compact as compared to the accretion disk. On the long space-ground baseline, however, they produce fluxes comparable to the average flux from the disk (see

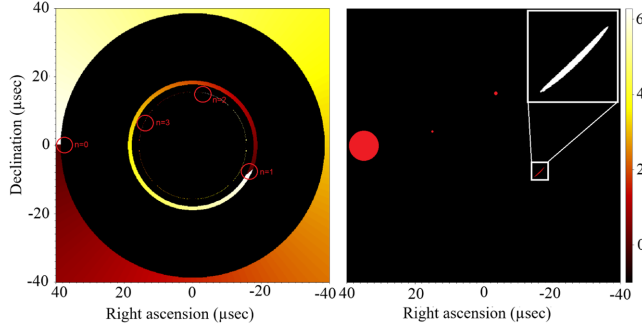


FIG. 3. On the left panel small red circles show: location of a flare spot in a selected region at the boundary between the bright and dim areas of the disk, and location of its reflections on the rings $n = 1, 2$ and 3 . The brightest and widest ring is the leading one with $n = 1$, the subring with $n = 2$ is seen as a very thin ring inward, the $n = 3$ subring further inward is not resolved in this figure. As in Fig. 2, the colors code the angular position on the disk. On the right panel we show the flare position on the accretion disk as a uniform red spot. It reflects on photon rings as spots of progressively smaller size, as seen on the right panel. The small filled circles on the right show the images of reflections on the observer's plane. The $n = 1$ reflection is shown in its real shape. Reflections with $n = 2$ and $n = 3$ are plotted schematically as small red points at their positions. In the upper right corner the shape of $n = 1$ reflection is shown at a larger scale. The total brightness of each n th order subring is ≈ 0.1 of the previous $(n - 1)$ th one [10].

discussion below). This circumstance can facilitate better observability of the photon ring and subrings on a short time scale. A very recent study Ref. [26] explores in detail how such reverberation of sporadic brightness variability in the accretion disk on photon rings manifests in single-dish observations.

Flares of brightness in the NIR and submm wavelength domains are observed in Sgr A*. Their duration varies from a few minutes, with a median delay of ~ 20 min in the submm to NIR [14,27,28], to ~ 1 –4 hours [29–33]. In millimeter (mm) and submm wavebands, the relative magnitude of variability of Sgr A*, i.e., the ratio of the observed peak to the minimum flux F_{\max}/F_{\min} , can reach the order of ~ 2 [14,33–36]. At higher frequencies this ratio increases approximately as $F_{\max}/F_{\min} \propto \nu^{1/2}$ as inferred in Ref. [15], see their Fig. 31.

The origin of these flares is still unclear, and possible mechanisms are widely debated (see discussions in Ref. [37]). Recently discussed related mechanisms include flarings from magnetic reconnection with associated flux eruptions [38–41] in the regime of a magnetically arrested accretion disk (MAD) in a near-horizon domain, $r \sim (10 - 40)r_g$ [17,42,43]. Lack of powerful reconnections in a standard accretion and normal evolution (SANE) model makes it inefficient in producing bright flares at high frequencies $\nu > 10^{14}$ Hz, as recently confirmed by Ref. [44]. Within the concept of MAD flows, the

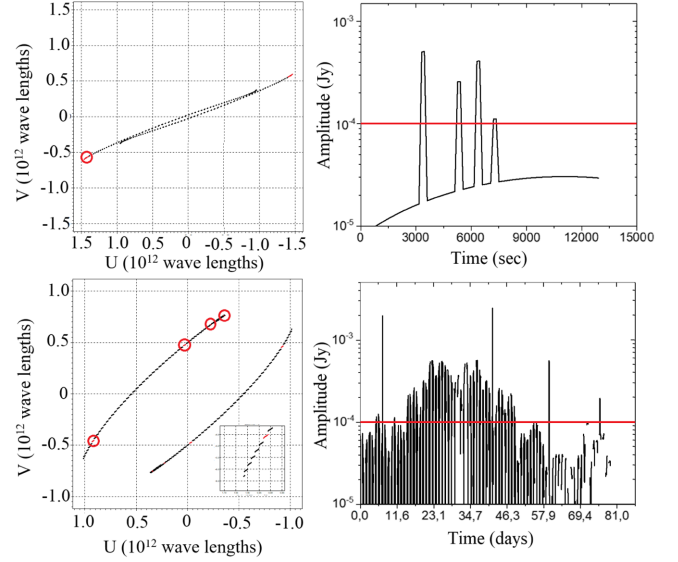


FIG. 4. The left panels show a typical uv coverage that will be available with the ALMA-MSO interferometer in the orbit around the L2 point. The right panels show the time dependence of the visibility amplitude for short flares as if they occurred in the accretion disk as shown schematically in Fig. 3. The upper row shows the case of Sgr A*, the lower row shows the case of M87*. The visibility function has been synthetically measured in the time range of approximately 60 full days for M87 and approximately 1 hour for Sgr A*. Open circles on the UV-tracks on the left panels indicate the times corresponding to the flare and its echoes. The total disk flux (i.e., the flux from $n = 0$ th order ring) is normalized to 1 Jy, flare magnitude in the disk is set to 2 Jy. The thick horizontal line in the right panels shows the 0.1 mJy sensitivity level (1σ) planned for the ALMA-MSO baseline.

characteristic time and scale are determined by the reconnection rate and the time of a few r_g/c needed for reestablishing the quasisteady-state accretion after the flare [42], in accordance with polarimetric measurements of the horizon scale $r \sim (6 - 10)r_g$ magnetic field in Sgr A* by the GRAVITY observations [45].

In the case of Sgr A*, stellar winds from Wolf-Rayet stars within the central parsec (from ~ 1 pc in the outer disk toward $\sim 300 r_g$ in the inner domain of the Galactic Center) can be an important source of maintaining MAD accretion [46–51]. Reference [52] presented a model of a stellar wind-fed MAD in Sgr A* that matches observational data and the time variability of rotation and dispersion measures, among other things (see Ref. [49] for more discussion and references). Previous estimates and conclusions that the flares are compact with sizes much less than the accretion disk, are largely consistent with these predictions. Reference [53] put an upper limit for their sizes $\lesssim 4r_g$. Reference [54] argued that a reasonable estimate from time delay between submm, near-infrared and x-ray can be $\approx 2r_g$. Recently Ref. [36] scrutinized a submillimeter flare in Sgr A*, and concluded from time-delay between

submillimeter and infrared that it is connected with a plasma blob of size $\sim r_g$. Even longer submm flares with $\Delta t \sim 1$ hour can be confined into compact regions of order $\sim r_g$ if the emitting plasma blobs expand adiabatically at a speed of $v \sim 0.005c$, as shown by Ref. [32]. More recent GRAVITY observations [45] spatially resolved three flaring blobs with orbital motions within $r \sim (6 - 10)r_g$ [40,55], i.e., close to the black hole. It is worth mentioning that even though the flares originate in the current sheet very close to or even partly within the ISCO region in the domain of jet formation, some of plasmoid blobs and associated flares still remain on stable orbits around the disk, as demonstrated by the GRAVITY experiment [45], and as such are not channeled into the jet.

A. Interferometer visibility function for a single flare

Asymptotically, the partial contribution of a photon ring with a given n into the visibility function at a baseline longer than $u \gg w_n^{-1}$ decays as $\propto u^{-1/2} e^{(-uw_n)^\zeta}$. Here, w_n is the width of n th ring, and ζ is determined by the radial profile of the photon ring [10]. Evidently, photon rings with smaller n and hence larger w_n decay faster. In our model, the visibility function on longer baselines for a uniform ring of a finite width w_n is determined directly as [56]

$$V_n(u) = \frac{1}{\pi d_n w_n u} (b_n J_1(2\pi b_n u) - a_n J_1(2\pi a_n u)), \quad (5)$$

where a_n is the inner, and b_n the outer radius of n th ring, $d_n = a_n + b_n$, and $b_n - a_n = w_n$, the width of the ring. As a consequence, on longer baselines the visibility amplitudes V_n with higher n become distinguishable from the amplitudes of the leading one, V_1 : at $u \sim 10 G\lambda$, the subring with $n = 2$ dominates, while at $u > 1000 G\lambda$, the subring $n = 3$ comes into play, as seen in Fig. 5. It is clearly seen though that the amplitude of the visibility function at long baselines declines dramatically and can fall below the sensitivity threshold of the instrument under use. Indeed, for M87*, with the central flux density of ~ 1 Jy, photon rings with $n = 3$ asymptotically decay by at least a factor of 30, and hence they cannot be resolved by the currently used or planned instruments, as seen in Fig. 5.

An alternative can be found in S-EVLBI observations of sufficiently bright flares in the accretion disk. Figure 5 also shows projections on U and V of the visibility function corresponding to the reflection of a single flare in the accretion disk on the corresponding photon ring. The flare compactness results in very compact echoes on rings, as seen in the ray-tracing shape of the $n = 1$ reflection in the upper right corner of Fig. 3. Therefore, despite the fact that the total flare flux is only twice the total flux from the entire quiet disk, its response seen in the amplitude of the visibility function on long interferometer baselines can be more than an order of magnitude higher than the visibility function of the corresponding ring. Thus, observation of

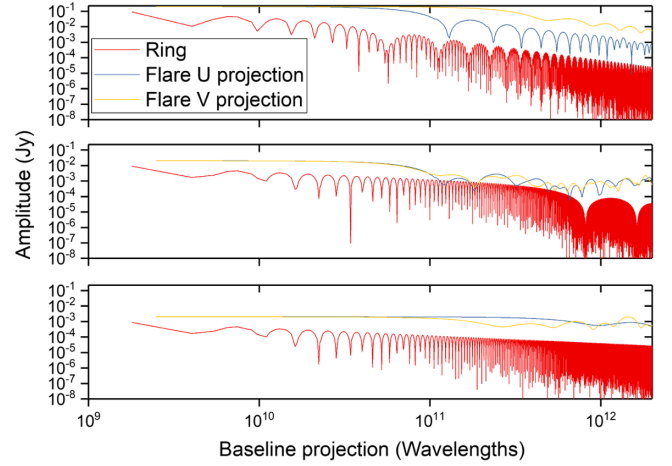


FIG. 5. 1D visibility functions V along u and v , panels from top to bottom show responds of different orders $n = 1, 2, 3$ from the photon rings themselves (lower curves) and the flares (upper curves): the darker (blue) lines present u -projections, whereas the pale (yellow) ones correspond to v -projections). The baseline is given in wavelengths, the total flux from the ring $n = 0$ (accretion disk) is normalized to 1 Jy; that from the flare in the disk $n = 0$ is normalized to 2 Jy; based on Ref. [10] we assume the total flux for each $n > 0$ to be 10% of the previous one $n - 1$.

VLBI flare signatures with long space-ground baselines requires an order of magnitude softer sensitivity requirements than those for observation of VLBI photon ring signatures from a smooth quiet disk.

B. Time variability of interferometer visibility function for a flare

Let us assume that a spatially localized short-term flare of $\Delta t_f < 5\pi r_g/c$ has occurred on the disk (see left panel on Fig. 3). The flare image reflects subsequently onto photon rings (Fig. 3), with the time gap between the subsequent subflares Δt_g nearly equal to $\sim 5\pi r_g/c$. The flare on the disk will first manifest in the visibility function in the central domain of u , and afterwards, with a time delay $\delta t_d \sim \Delta t_g$, it will subsequently appear in the peripheral domains of u corresponding to photon rings with an increasing n . The exact value of δt_d was calculated from the model using ray tracing. The advantage related to such manifestations is that each subflare on the corresponding subring does appear separately of the previous brighter subflare, and thus can be distinguished easier. An example of how a flare on the disk will reverberate on the visibility function with the ALMA-MSO S-VLBI is demonstrated in Fig. 4. The left panels show a typical uv coverage expected within ALMA-MSO interferometric observations of Sgr A* (top row) and M87* (bottom row) in orbit around the L2 point. The right panels show the time dependence of the measured visibility amplitude for short flares. For the flares, we assume the magnitude of twice the steady state accretion disk [14], i.e., 2 Jy for Sgr A*. Figure 5 depicts 1D visibility functions for

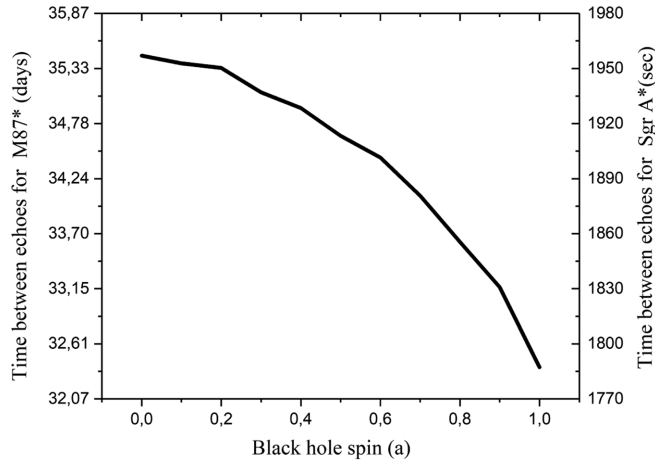


FIG. 6. The plot shows time delay between the flares in the third and the first photon rings Δt versus the black hole spin for M87* (left y-axis) and Sgr A* (right y-axis), $\theta_{\text{los}} = 0$. Relativity short ($\lesssim 1$ hour for Sgr A* and $\lesssim 3$ days for M87*) flux monitoring is sufficient for the flare echoes to be distinguished.

the flare schematically shown in Fig. 3 and subsequently reflected on subrings $n = 1, 2, 3$ (top to bottom). Lower curves in the panels show visibility functions $V(u)$ of subrings from a quiet disk, the upper curves correspond to visibility functions $V(u)$ (blue) and $V(v)$ (yellow) in u and v projections, respectively. As seen, the amplitude of the visibility function of echoes from the flare on the long space-ground baseline is more than an order of magnitude higher than the one of the corresponding ring itself, because of the compactness of the flare compared to the disk. This results in an order of magnitude weaker sensitivity requirements for the detection of VLBI flare signatures with long space-ground baselines than sensitivity needed to detect VLBI photon ring signatures from a smooth quiet disk.

The time lag between the arrival times of the echo from the flare in the first and subsequent rings can be used to determine the parameter a . Figure 6 shows the time delay between the flare copies in the third and the first photon rings versus the black hole spin for M87* and Sgr A*. Due to the mass difference the reverberation time lag between the echoes in the first and third ring in the case of M87* is considerably longer—about 30 days as compared with the short lag \lesssim several minutes in Sgr A*, and seems sufficient for monitoring the reverberation on a known date (within $\lesssim 3$ days window for M87*) with the S-E VLBI baseline in both cases. For instance, in the case of Sgr A*, flux monitoring for about 2 hours can bring a pronounced conclusive result.

C. Angular displacements of the VLBI flare image for Sgr A*

Longer submm flares in Sgr A* with $\Delta t_f > 5\pi r_g/c$ can be represented in the VLBI image as a superposition of the flare in the accretion disk and its echoes on the photon

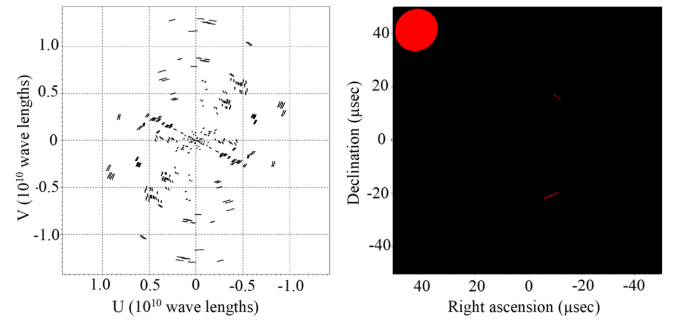


FIG. 7. Left panel: UV-coverage for a synthetic instantaneous ngEHT observation of Sgr A*. Duration of observations is assumed 30 minutes, UV plane coverage is composed for two frequencies 230 and 340 GHz, the sites and parameters of the ngEHT array are taken from Ref. [57]. Right panel: VLBI model image for a long flare. It consists of a flare in the thin accretion disk with a total flux of 2 Jy and two echoes in the photon rings. The total flux in the first echo is 0.2 Jy and 20 mJy in the second one, the black hole spin is taken $a = 0.8$, the inclination angle $\theta_{\text{los}} = 0$. Model image is obtained by ray tracing.

rings. An example of a synthetic observation with the ngEHT array is shown on the right panel of Fig. 7. The left panel of Fig. 7 shows the UV-coverage for a synthetic “instantaneous” ngEHT observation of Sgr A* for 30 minutes. The UV plane coverage is composed of two frequencies 230 and 340 GHz. The sites and parameters of the ngEHT array are taken from Ref. [57]. The right panel of this figure presents the VLBI model image of a long flare. The image shows a flare in the thin accretion disk with a total flux of 2 Jy [14] and two echoes in the photon rings. The total flux in the first echo is 0.2 Jy and in the second echo 20 mJy. Black hole spin $a = 0.8$, $\theta_{\text{los}} = 0$. The model image was obtained by ray tracing. In Sgr A*, the characteristic time of long flares in millimeter wavelengths is 30 min—2 hours [58], at least ten times longer than the gravitation time ~ 200 s. Therefore, for Sgr A*, several bright spots will be simultaneously visible in the VLBI image (see the right panel of Fig. 7 and the left panel of Fig. 8). The relative positions of these bright spots can be used to directly determine the parameters a and θ_{los} . It is important to note that the angular resolution of the ground VLBI is sufficient to accurately determine the coordinates of bright spots in the image, provided that the UV-plane has a good filling and the array ensures good sensitivity, as planned in the ngEHT. Figure 8 (left panel) shows the reconstructed instantaneous VLBI image by the CLEAN method. The white lines mark the angle α between the direction of the flare in the accretion disk and the direction of its echo in the $n = 1$ photon ring. The intensity (Jy/beam) is plotted in logarithmic scale. The right panel shows the dependence of the angle α on the black hole spin parameter a . The positions of the spots in the VLBI image were assumed to coincide with intensity maximums. The broken line corresponds to the restored ngEHT VLBI

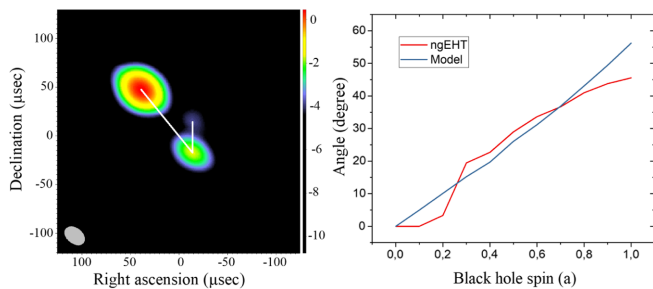


FIG. 8. Left panel: reconstructed instantaneous VLBI image of a long flare in the accretion disk and two echoes in the photon ring with the ngEHT VLBI array by CLEAN method. The lower left corner shows the beam size, the array parameters are taken from Ref. [57], UV-coverage and source model are plotted at Fig. 7. White lines mark the angle α between the direction of the flare in the accretion disk and the direction of its echo in the $n = 1$ photon ring, the intensity is plotted in logarithmic scale (Jy/beam). Right panel: dependence between the angle α and the black hole spin a . The positions of the spots on the VLBI image are determined from the intensity maximum. The broken line corresponds to the restored ngEHT VLBI image, the straight one corresponds to the model. As seen, the angular resolution and 30-minutes UV-coverage of the ngEHT is sufficient to measure the angle α .

image, the straight line is from the model. The sensitivity provided by a key anchor station of the ngEHT jointly with a small 10-m dish is about 5–20 mJy (Fig. 7 in Ref. [57]), which corresponds to 2 GHz bandwidth and a few seconds atmospheric timescale. The planned bandwidth in the ngEHT is 16 GHz, so it will improve the sensitivity $\approx \sqrt{16 \text{ GHz}/2 \text{ GHz}} \approx 2.8$ times. Simultaneous observations at two frequencies using the FPT technique [59] will increase the currently short coherence time of a few seconds (due to atmosphere) to about 150 s (due to the H-maser stability on the site). Thus, theoretically the VLBI sensitivity can be increased $\approx \sqrt{150 \text{ s}/3 \text{ s}} \approx 7$ times more, and one may conclude that the planned ngEHT sensitivity will be sufficient to detect bright spots in the accretion disk and their echoes on the first and the second photon rings.

V. SUMMARY

In this paper, we analyzed a feasibility to observe manifestations of photon rings around the shadow of a supermassive black hole and to obtain information about the spacetime metric. Within a simplified model we showed that

- (1) SE-VLBI observations with the joint EHT-MSO program seem promising to detect manifestations

of photon rings $n = 1, 2$ from bright (with a factor of 2 magnitude enhancement) flares, provided that the maximum visibility function $V(0) \approx 1 \text{ Jy}$, as for M87* [6]. Generally, the signal can be distinguished on baselines achievable by the joint EHT-MSO observations with the anticipated 1σ sensitivity $\delta S \sim 0.1\text{--}0.3 \text{ mJy}$ at the Lagrange libration point L2 with $u \sim 1 \text{ T}\lambda$ [13]. Despite the fact that the total flare flux is only twice the total flux from the corresponding ring, on a long interferometer baseline the flare can give more than an order of magnitude greater amplitude of the visibility function due to the fact that the flare itself concentrates the emission flux comparable to that from the entire disk, and the echo from the flare on the ring is much more compact than the respective ring. Thus, observation of VLBI flare signatures with long space-ground baselines requires an order of magnitude softer sensitivity requirements than observation of VLBI photon ring signatures from a quiet disk.

- (2) The brightness distribution on photon rings reflects the disk brightness with a time delay. The short strong flare in M87* and Sgr A* observed on long EHT-MSO baseline produces a series of subflares on photon rings with definite time delays between them. The relative times between the subflares provide a possibility to directly determine the parameters a and θ_{los} of the black hole.
- (3) The brightness distribution on photon rings reflects the disk brightness with an angular displacement. As a result, a single flare on the disk can produce several bright spots on photon subrings with a short time delay Δt_f in the VLBI image. From the relative positions of these spots, one can directly determine the parameters a and θ_{los} of the black hole. The angular resolution, the quality of 30-min UV-coverage and the sensitivity of the ground-based ngEHT are sufficient to resolve at least three (one in the accretion disk and two in the subring reflections) of these bright spots in Sgr A*.

ACKNOWLEDGMENTS

S. V. C. was supported by RFBR Grant No. 20-02-00469. The work of Y. S. is done under partial support from the project “New Scientific Groups of Lebedev Physical Institute” 41-2020 financed by the Ministry of Education and Science of Russian Federation.

- [1] Event Horizon Telescope Collaboration, *Astrophys. J. Lett.* **875**, L1 (2019).
- [2] Event Horizon Telescope Collaboration, *Astrophys. J. Lett.* **875**, L2 (2019).
- [3] Event Horizon Telescope Collaboration, *Astrophys. J. Lett.* **875**, L3 (2019).
- [4] Event Horizon Telescope Collaboration, *Astrophys. J. Lett.* **875**, L4 (2019).
- [5] Event Horizon Telescope Collaboration, *Astrophys. J. Lett.* **875**, L5 (2019).
- [6] Event Horizon Telescope Collaboration, *Astrophys. J. Lett.* **875**, L6 (2019).
- [7] H. Falcke and S. B. Markoff, *Classical Quantum Gravity* **30**, 244003 (2013).
- [8] H. Falcke, F. Melia, and E. Agol, *Astrophys. J. Lett.* **528**, L13 (2000).
- [9] K. Gebhardt, J. Adams, D. Richstone, T. R. Lauer, S. M. Faber, K. Gültekin, J. Murphy, and S. Tremaine, *Astrophys. J.* **729**, 119 (2011).
- [10] M. D. Johnson, A. Lupsasca, A. Strominger, G. N. Wong, S. Hadar, D. Kapec, R. Narayan, A. Chael, C. F. Gammie, P. Galison, D. C. M. Palumbo, S. S. Doeleman, L. Blackburn, M. Wielgus, D. W. Pesce, J. R. Farah, and J. M. Moran, *Sci. Adv.* **6**, eaaz1310 (2020).
- [11] J. M. Bardeen, in *Black Holes (Les Astres Occlus)* (1973), pp. 215–239, <https://ui.adsabs.harvard.edu/abs/1973blho.conf..215B/abstract>.
- [12] J. P. Luminet, *Astron. Astrophys.* **75**, 228 (1979).
- [13] I. D. Novikov *et al.*, *Phys. Usp.* **64**, 386 (2021).
- [14] G. Witzel, G. Martinez, S. P. Willner *et al.*, *Astrophys. J.* **917**, 73 (2021).
- [15] R. Genzel, F. Eisenhauer, and S. Gillessen, *Rev. Mod. Phys.* **82**, 3121 (2010).
- [16] L. Murchikova and G. Witzel, *Astrophys. J. Lett.* **920**, L7 (2021).
- [17] B. Ripperda, F. Bacchini, and A. A. Philippov, *Astrophys. J.* **900**, 100 (2020).
- [18] K. Chatterjee, S. Markoff, J. Neilsen *et al.*, *Mon. Not. R. Astron. Soc.* **507**, 5281 (2021).
- [19] G. C. Debney, R. P. Kerr, and A. Schild, *J. Math. Phys. (N.Y.)* **10**, 1842 (1969).
- [20] R. P. Kerr and A. Schild, in *IV Centenario Della Nascita di Galileo Galilei, 1564–1964* (1965), p. 222, <https://ui.adsabs.harvard.edu/abs/1965cngg.conf..222K/abstract>.
- [21] H. Balasin and H. Nachbagauer, *Classical Quantum Gravity* **11**, 1453 (1994).
- [22] A. Krasinski, E. Verdaguer, and R. P. Kerr, *Gen. Relativ. Gravit.* **41**, 2469 (2009).
- [23] C. T. Cunningham and J. M. Bardeen, *Astrophys. J.* **183**, 237 (1973).
- [24] S. E. Gralla, D. E. Holz, and R. M. Wald, *Phys. Rev. D* **100**, 024018 (2019).
- [25] S. E. Gralla and A. Lupsasca, *Phys. Rev. D* **101**, 044031 (2020).
- [26] P. M. Chesler, L. Blackburn, S. S. Doeleman, M. D. Johnson, J. M. Moran, R. Narayan, and M. Wielgus, *Classical Quantum Gravity* **38**, 125006 (2021).
- [27] K. Dodds-Eden *et al.*, *Astrophys. J.* **698**, 676 (2009).
- [28] T. Do, G. Witzel, A. K. Gautam, Z. Chen, A. M. Ghez, M. R. Morris, E. E. Becklin, A. Ciurlo, J. Hosek, Matthew G. D. Martinez, K. Matthews, S. Sakai, and R. Schödel, *Astrophys. J. Lett.* **882**, L27 (2019).
- [29] J. C. Mauerhan, M. Morris, F. Walter, and F. K. Baganoff, *Astrophys. J. Lett.* **623**, L25 (2005).
- [30] D. P. Marrone, J. M. Moran, J.-H. Zhao, and R. Rao, *Astrophys. J.* **640**, 308 (2006).
- [31] D. P. Marrone, F. K. Baganoff, M. R. Morris, J. M. Moran, A. M. Ghez, S. D. Hornstein, C. D. Dowell, D. J. Muñoz, M. W. Bautz, G. R. Ricker, W. N. Brandt, G. P. Garmire, J. R. Lu, K. Matthews, J. H. Zhao, R. Rao, and G. C. Bower, *Astrophys. J.* **682**, 373 (2008).
- [32] A. Eckart *et al.*, *Astron. Astrophys.* **492**, 337 (2008).
- [33] G. Trap, A. Goldwurm, K. Dodds-Eden, A. Weiss, R. Terrier, G. Ponti, S. Gillessen, R. Genzel, P. Ferrando, G. Bélanger, Y. Clénet, D. Rouan, P. Predehl, R. Capelli, F. Melia, and F. Yusef-Zadeh, *Astron. Astrophys.* **528**, A140 (2011).
- [34] J.-H. Zhao, K. H. Young, R. M. Herrnstein, P. T. P. Ho, T. Tsutsumi, K. Y. Lo, W. M. Goss, and G. C. Bower, *Astrophys. J. Lett.* **586**, L29 (2003).
- [35] J. Dexter, B. Kelly, G. C. Bower, D. P. Marrone, J. Stone, and R. Plambeck, *Mon. Not. R. Astron. Soc.* **442**, 2797 (2014).
- [36] J. M. Michail, M. Wardle, F. Yusef-Zadeh, and D. Kunneriath, *Astrophys. J.* **923**, 54 (2021).
- [37] M. García-Marín *et al.*, *Astrophys. J.* **738**, 158 (2011).
- [38] J. Dexter, A. Tchekhovskoy, A. Jiménez-Rosales, S. M. Ressler, M. Bauböck, Y. Dallilar, P. T. de Zeeuw, F. Eisenhauer, S. von Fellenberg, F. Gao, R. Genzel, S. Gillessen, M. Habibi, T. Ott, J. Stadler, O. Straub, and F. Widmann, *Mon. Not. R. Astron. Soc.* **497**, 4999 (2020).
- [39] E. Petersen and C. Gammie, *Mon. Not. R. Astron. Soc.* **494**, 5923 (2020).
- [40] O. Porth, Y. Mizuno, Z. Younsi, and C. M. Fromm, *Mon. Not. R. Astron. Soc.* **502**, 2023 (2021).
- [41] E. M. Gutiérrez, R. Nemmen, and F. Cafardo, *Astrophys. J. Lett.* **891**, L36 (2020).
- [42] B. Ripperda, M. Liska, and K. E. A. Chatterjee, *Astrophys. J. Lett.* **924**, L32 (2022).
- [43] A. Chashkina, O. Bromberg, and A. Levinson, *Mon. Not. R. Astron. Soc.* **508**, 1241 (2021).
- [44] N. Scepi, J. Dexter, and M. C. Begelman, *Mon. Not. R. Astron. Soc.* **511**, 3536 (2022).
- [45] R. Abuter, A. Amorim, M. Bauböck, and E. A. Berger (Gravity Collaboration), *Astron. Astrophys.* **618**, L10 (2018).
- [46] J. Cuadra, S. Nayakshin, and F. Martins, *Mon. Not. R. Astron. Soc.* **383**, 458 (2008).
- [47] J. Cuadra, S. Nayakshin, and Q. D. Wang, *Mon. Not. R. Astron. Soc.* **450**, 277 (2015).
- [48] S. M. Ressler, E. Quataert, and J. M. Stone, *Mon. Not. R. Astron. Soc.* **478**, 3544 (2018).
- [49] S. M. Ressler, E. Quataert, and J. M. Stone, *Mon. Not. R. Astron. Soc.* **492**, 3272 (2020).
- [50] S. M. Ressler, C. J. White, E. Quataert, and J. M. Stone, *Astrophys. J. Lett.* **896**, L6 (2020).
- [51] D. Calderón, J. Cuadra, and E. A. Schartmann, *Astrophys. J. Lett.* **888**, L2 (2020).
- [52] S. M. Ressler, E. Quataert, and J. M. Stone, *Mon. Not. R. Astron. Soc.* **482**, L123 (2019).

- [53] S. S. Doeleman *et al.*, *Nature (London)* **455**, 78 (2008).
- [54] G. Witzel, G. Martinez, J. Hora, S. P. Willner, M. R. Morris, C. Gammie, E. E. Becklin, M. L. N. Ashby, F. Baganoff, S. Carey, T. Do, G. G. Fazio, A. Ghez, W. J. Glaccum, D. Haggard, R. Herrero-Illana, J. Ingalls, R. Narayan, and H. A. Smith, *Astrophys. J.* **863**, 15 (2018).
- [55] D. Ball, F. Özel, P. Christian, C.-K. Chan, and D. Psaltis, *Astrophys. J.* **917**, 8 (2021).
- [56] S. V. Chernov, *J. Exp. Theor. Phys.* **132**, 897 (2021).
- [57] L. Blackburn, S. Doeleman, and J. Dexter *et al.*, [arXiv:1909.01411](https://arxiv.org/abs/1909.01411).
- [58] F. Yusef-Zadeh, M. Wardle, C. Heinke, C. D. Dowell, D. Roberts, F. K. Baganoff, and W. Cotton, *Astrophys. J.* **682**, 361 (2008).
- [59] G.-Y. Zhao, J. C. Algaba, S. S. Lee, T. Jung, R. Dodson, M. Rioja, D.-Y. Byun, J. Hodgson, S. Kang, D.-W. Kim, J.-Y. Kim, J.-S. Kim, S.-W. Kim, M. Kino, A. Miyazaki, J.-H. Park, S. Trippe, and K. Wajima, *Astron. J.* **155**, 26 (2018).